This document is the accepted manuscript version of the following article:

Srivastava, G., Štacko, P., Mendieta-Moreno, J. I., Edalatmanesh, S., Kistemaker, J. C. M., Heideman, G. H., … Ernst, K. H. (2023). Driving a third generation molecular motor with electrons across a surface. ACS Nano, 17(4), 3931-3938. https://doi.org/10.1021/acsnano.2c12340

Driving a 3rd Generation Molecular Motor with Electrons Across a Surface

Gitika Srivastava,[†] Peter Štacko,[‡] Jesús I. Mendieta-Moreno,[&] Shayan Edalatmanesh,[&] Jos C. M. Kistemaker,[‡] G. Henrieke Heideman,[‡] Laura Zoppi,[†] Manfred Parschau,[†] Ben L. Feringa[‡,] and Karl-Heinz Ernst[†,&,#,]**

[†] Molecular Surface Science and Coating Technology Laboratory, Empa, Swiss Federal Laboratories for Materials Science and Technology, Überlandstrasse 129, 8600 Dübendorf

[‡] Centre for Systems Chemistry, Stratingh Institute for Chemistry and Zernike Institute for Advanced Materials, University of Groningen, Nijenborgh 4, 9747 AG Groningen, Netherlands

[&] Nanosurf Laboratory, Institute of Physics, The Czech Academy of Sciences, Cukrovarnická 10, 162 00 Prague, Czech Republic

[#] Department of Chemistry, University of Zurich, Winterthurerstrasse 190, 8057 Zürich, Switzerland

E-mails: karl-heinz.ernst@empa.ch; b.l.feringa@rug.nl

ABSTRACT Excitation of single molecules with electrons tunneling between a sharp metallic tip of a scanning tunneling microscope and a metal surface is one way to study and control dynamics of molecules on surfaces. Electron tunneling induced dynamics may lead to hopping, rotation,

molecular switching, or chemical reactions. Molecular motors that convert rotation of subgroups into lateral movement on a surface can in principle also be driven by tunneling electrons. For such surface-bound motor molecules the efficiency of motor action with respect to electron dose is still not known. Here, the response of a molecular motor containing two rotor units in form of overcrowded alkene groups to inelastic electron tunneling has been examined on a Cu(111) surface in ultrahigh vacuum at 5 K. Upon vibrational excitation, switching between different molecular conformations is observed, including conversion of enantiomeric states of chiral conformations. Tunneling at energies in the range of electronic excitations causes activation of motor action and to movement across the surface. The expected unidirectional rotation of the two rotor units causes indeed forward movements but with a low degree of translational directionality.

KEYWORDS

chirality, molecular motors, STM, single molecule studies, molecular dynamics

Directionality of motion is fundamentally important for the functioning of biological molecular motors[1] and key to future artificial molecular machines.[2-15] Providing continuous directional motions upon external stimuli, artificial molecular motors have become a prominent area in chemical sciences enabling the transition to dynamic molecular systems and responsive materials.[2-15] In particular overcrowded alkenes have attracted considerable attention due to their repetitive rotation upon light irradiation.[16-18] Followed by *E*-*Z* isomerization of the alkene group, a vibrationally-induced helix inversion leads basically to rotation of 180° of one part of the molecule with respect to the other (Figure 1). Directionality of artificial motors has originally been introduced by installing chirality into the molecular machine, rendering the potential energy surface (PES) of the excited state asymmetric.[19,20] As a consequence, a ratchet-shaped energy

landscape of the process is induced.[21] However, it has also been shown that chirality is non-essential for directionality, provided control over the sequence of steps inducing rotation is secured.[22-26]

As the founding technique of nanotechnology, scanning tunneling microscopy (STM) has been developed well beyond a plain tool for imaging.[27] Manipulation of single atoms and molecules with the STM tip is a well-established procedure nowadays,[28,29] and has been utilized, for example, for lateral separation of enantiomers at the nanoscale.[30,31] The STM instrument has also been used for studying molecular surface dynamics after vibrational excitation of small single molecules, such as carbon monoxide, propene and acetylene.[32-34] The advantage of this approach is the possibility that the molecule can become excited by means of inelastic electron tunneling (IET) and the type of response is directly analyzed by microscopy. A variety of different molecular dynamic modes has been identified,[35] such as rotation,[33,36-37] translation,[32,33] desorption,[38] chemical reactions,[39-41] and switching.[42-44] By using chiral molecules or a chiral surface a preferred sense of rotation for small molecules on surfaces has been realized.[45-47]

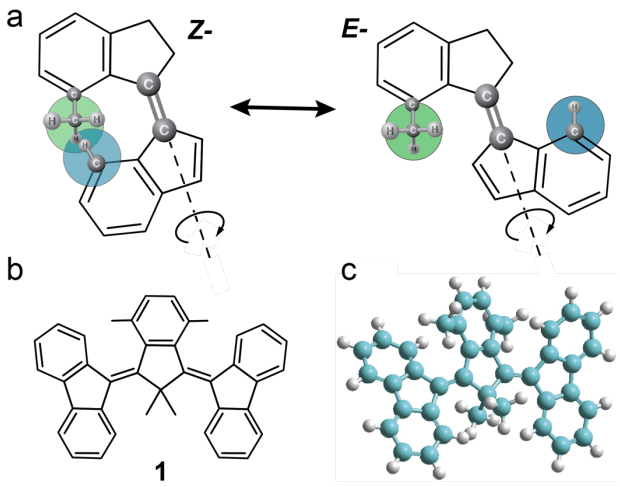

Figure 1. a) Principle of *E-Z* isomerization of an overcrowded alkene. Steric hindrance of parts of the molecule (semitransparent filled circles) imposes torsion to the alkene double bond and installs helical chirality. After *E-Z* isomerization one end at the alkene group has been rotated by 180°. b) Structure of 3rd-generation molecular motor. Due to the symmetric character of the two fluorenylene groups, the *E-Z* isomerization leads again to an overcrowded alkene. c) Ball-and-stick model of **1** demonstrating the overcrowded structure.

Besides by optical stimulus,[48,49] surface mounted molecular motors can also be driven by means of IET. The most prominent example is the nanocar, possessing four molecular rotors.[50] Initially, *E–Z* isomerization of rotor units was induced by electron tunneling from the STM tip, followed by their thermal helix inversion. This led to a small displacement of the molecule on the surface and multiple excitation steps caused movement across the surface with a high degree of directionality. It represented a good example in which directional rotation was turned into directional propulsion at the nanoscale.[50] However, details of the mechanism remain unclear while it will guide the design of future molecular propulsion systems and attempts to achieve control over translational movement. Of particular interest is the role of chirality and the efficacy of motor action with respect to the number of injected electrons.

Here, the movement of a two-rotor motor molecule (Figure 1) on a copper(111) surface with inelastically tunneling electrons is reported. The molecule is based on a 3rd generation motor featuring two sterically overcrowded alkenes and may exist in different helical conformations.[51,52] Although achiral in its stable meso forms, the helical structure of its two halves installs local asymmetry at both sides of the molecule.[51] It is found here that vibrational IET excitation induces conformational switching while electronic excitation causes E-Z isomerization leading to movement of the molecule across the surface.

RESULTS AND DISCUSSION

Conformational switching by vibrational excitation

In order to analyze the switching between different conformations *via* helix inversion of a single molecule, at first theoretical evaluations of different conformers and their STM appearance are presented. (Note that upon electronic excitation *E*-*Z* isomerization is included in the interconversion of the isomers. However, as the four isomers of **1** can be interconverted without any bond-breaking they are therefore not called 'configurations' here.) Previous work for the free molecule revealed that these motors have access to four distinguishable conformations, two helical enantiomers and two *meso* isomers.[51] In the enantiomers both halves have identical sense of helicity, i.e., either *(P,P)* or *(M,M)*, while the two *meso* forms have *(M,P)* and *(P,M)* conformation. These four diastereomers are represented here as *(P)*-**1** and *(M)*-**1** and as *meso*-**1** and *meso*-**1'**, respectively.[51] Accordingly, four different STM contrasts for individual molecules were indeed observed. Figure 2 shows three experimental STM images as well as the calculated STM constant current contrast for the *meso*-isomers and the *(P)*-**1** enantiomer. A mirror-like appearance of what has been assigned in Figure 2 as *(P)*-**1** enantiomer is shown in Figure S1 and represents therefore the *(M)*-**1** enantiomer. Note that this particular *(M)*-**1** enantiomer has been directly created by conformational switching from the *(P)*-**1** enantiomer. Support for the initial assignment presented in Figure 2 comes also from the fact that the STM contrasts of the two meso isomers exhibit mirror symmetry.

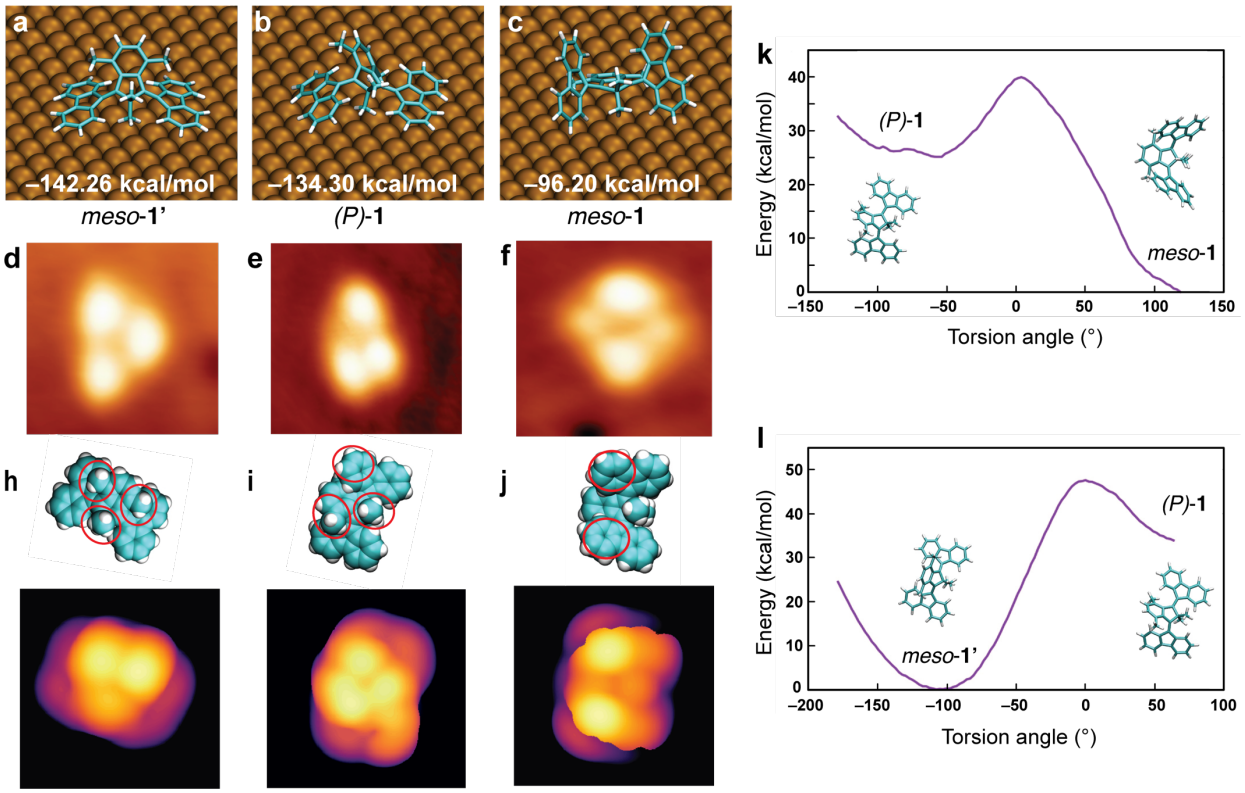

Figure 2. Different conformations of **1** at the surface and their STM contrasts. a,b,c) Conformations of **1** on the Cu(111) surface. Not shown is the *(M)*-**1** enantiomer. Due to the larger contact surface area *meso*-**1'** is the lowest energy conformation. d,e,f) Experimental ST micrographs (3.3 nm × 3.3 nm, 50 mV, 10 pA). h,i,j) Molecular conformations and calculated STM contrast (3.0 nm × 3.0 nm, height span from black to white 1.7 nm) of three conformers. The parts of the molecule that contribute most to the contrast are marked by red ellipses. k,l) Inversion barriers for conversion of *(P)*-**1** into *meso*-**1** and *meso*-**1'** into *(P)*-**1** as obtained by molecular dynamics calculations.

For the theoretical evaluation, three conformers have been relaxed by DFT, while the interaction with the surface has been evaluated with the force-field approach (Figure 2a-c). The comparison of structures of *(P)*-**1** (Figure 2b) and a fully DFT optimized *(P)*-**1** enantiomer on a four-layer Cu(111) slab (Figure S2) shows good agreement and justifies therefore the DFT/force field

(QM/MM) approach. The meso-**1'** adsorbate has the lowest energy on the surface, which is due to maximal van der Waals overlap of the fluorene groups with the surface (Figure 2a). As the high flexibility of this molecule supposedly leads to further structural changes in the tunnel junction, additional small conformational changes had to be considered in order to achieve reasonable agreement of experimental and theoretical STM contrast (Figure S3). That flexible molecules take different conformations in the tunnel junction than at the surface itself has, for example, been reported for molecular rotors previously.[53,54]

Under the here applied low bias tunneling conditions of only 50 mV, the STM contrast in constant current mode should be dominated by the distal parts of the conformers. These are the methyl groups for the *meso*-**1'**, the upper benzo tabs of the two fluorene groups in *meso*-**1**, and two methyl groups plus one benzo tab in the enantiomers. The tunnel contrast also depends on the tip condition, which is considered as s-orbital in the modelling. Hence, more features from the lower molecular parts are part of the theoretical contrast, which are not necessarily observed in the experimental contrasts.

In order to estimate the inversion barriers between the conformers in comparison with values obtained for the free molecule,[51] DFT calculations have been performed for the molecular frame while the interaction with the surface of at each state was calculated by Amber force fields. Except for the fixed dihedral angle between C-C bonds at the alkene group as reaction coordinate, the adsorbate at each step of the inversion was allowed to fully relax. Interestingly, the barriers for isomerization starting from *(P)*-**1** into *meso*-**1** and into *meso*-**1'** (15 and 20 kcal/mol, respectively. Figures 2k,l) are quite similar to the value for the free species of 19 kcal/mol.[51] This means that either the weak van der Waals interaction with the surface does not impose additional hinderance

or does even stabilize in part transition states. The values also show that conformational switching by vibrational excitation from IET is even at 5 K possible.

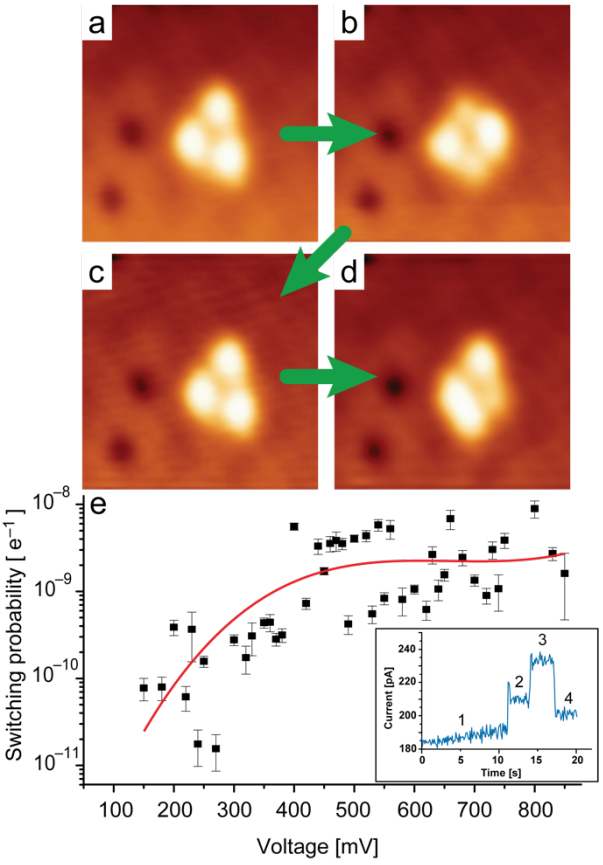

Figure 3. Conformational switching of a single motor molecule by inelastic electron tunneling. a) STM image of initial state of **1**. b-d) STM images after injection of electrons at U_{bias} = 400 mV, showing change of appearance. The two black dots in the images are carbon monoxide molecules adsorbed from the residual gas. Imaging parameters: 6 nm × 6 nm, 50 mV, 10 pA. e) Action spectrum of observed conformational changes. (Two events with probabilities of 1 × 10^{-12} per electron and 4 × 10^{-12} per electron at 350 mV and 380 mV are not shown. Error bars are the standard deviation of successful events. See Equation S1) The red curve represents the polynomial fit of all switching events. The inset shows the time-current trace of switching from 2a→2b. Besides initial (1) and final state (4) two intermediate conformations (2,3) are identified.

Having the different STM contrasts assigned to plausible conformations, the IET-induced conformation switching can be analyzed. Figure 3 shows STM images before and after injecting electrons of 400 meV energy into the molecule. More examples for conformational switching sequences are shown in Figure S4. Note that the switching procedure does not include any scanning of the tip (see methods section). Pushing and dragging of the molecule is therefore excluded and the conformational changes must be solely attributed to IET. Consequently, the position of the molecule does not really change upon conformational switching (Figure S1 & Figure S5). Other action modes such as hopping or rotation are not observed under the 'mild' conditions of IET applied for conformation switching. Moreover, the scanning conditions for analyzing the post-excitation state, i.e., low bias voltage and low tunneling current, were chosen such that no further switching occurred. Consequently, a change of STM appearance for the same molecule is only observed if a different conformation is taken after the voltage pulse.

The 3a→3b→3c switching processes illustrated in Figure 3 represents switching from one meso-form into the other, that is, meso-**1'**→ meso-**1** → meso-**1'**. The change documented by STM images 3c and 3d corresponds to switching the meso-**1'** conformation into the *(M)*-**1** enantiomer. However, the STM images represent the final state after the end of the voltage pulse and intermediate conformations cannot be excluded. For example, the time-current trace for the conversion from Figure 3a to Figure 3b (Figure 3e, inset) shows overall four current levels. Hence, two intermediate conformations must have been adopted. From the time-current traces (such as the one shown Figure 3e, inset), the probability of switching per tunneling electron has been calculated.

The origin of the conformation change is vibrational excitation by inelastically tunneling electrons. Although a vibrationally excited molecule on a metal surface usually cools down *via*

electron hole pair formation in the metal substrate within picoseconds,[55,56] for sufficient lifetimes of the vibrationally excited state a molecule can undergo an action, here the switching of conformation. However, after initial excitation of one vibrational mode, anharmonic coupling to other vibrational modes is expected, then leading to conformational switching.[35] Nevertheless, an exponential rise in probability at a certain threshold voltage may allow identification of the corresponding vibrational mode that became initially excited. In the case of the nanocar, conformational changes such as helix inversion have been observed from 200 mV bias voltage on, suggesting initial trigger by excitation of the C=C stretching vibration at 200 meV.[50] Ground-state Raman modes of the C=C part in a similar single rotor molecule are indeed located just below 200 meV.[57] For the 3rd generation motor molecule here, no switching event has been observed below 150 mV bias voltage and the probability rises roughly by a factor of 100 in the range between 200 and 400 mV (Figure 3e). This means that not a particular vibration excitation can be identified for the conformational change. Therefore, different vibrations may have become initially excited, including C-C stretching vibrations of the aromatic rings, the C=C stretching mode or C-H stretching vibrations in the methyl groups at 360 meV. Consequently, the action spectrum shown in Figure 3e represents many different types of conformational changes. As often multiple changes were observed in current-time traces without clear identification of the corresponding switching action (Figure 2e inset, Figure S2a), it was not possible to analyze the conformational switching for a defined initial conformation. In other cases, the STM contrast did not clearly allow correlation with a single configuration due to STM tip changes. As expected for vibrational IET excitation, no substantial differences in conformational switching are noted when tunneling of opposite bias has been performed. That is, for a conformational change it does not matter if the electrons tunnel from the metal tip to the copper surface or from the surface to the metal tip. Above 400 mV bias

voltage the switching probability has values of up to 10^{-8} per electron. Compared to other IET-induced molecular surface dynamics, this seems quite large. However, so far mostly dynamics of small molecules were investigated that are more tightly bound to the surface.[32-41] For IET-induced rotation of a ferrocene-armed rotor, a similar yield has been reported.[43]

Movement by motor action after electronic excitation

As already mentioned, no substantial lateral movement is observed upon conformational switching (Figure S5). As for the nanocar, movement of **1** across the surface was only observed at larger bias voltages. Figure 4 shows STM images after manipulation with 800 meV electrons. The movement is clearly recognized by the change in relative position to static co-adsorbed CO molecules (black dots). More moving events are documented in Figures S6 to S8. The correlation of the energetic onset of movement with the position of the unoccupied molecular states suggest that motor action is induced by electronic excitation. Although the projected density of states (Figure 4l) shows a shift of the LUMO from 800 meV to 900 meV for the free molecule to the adsorbed state, the onset starts already at about 750 meV, a value when first movement is experimentally observed (Figure 4m). With increasing bias voltage, the yield of movement increases by more than a factor of 10 (Figure 4m). The efficacy is roughly on the order of other IET-induced surface dynamics.[35]

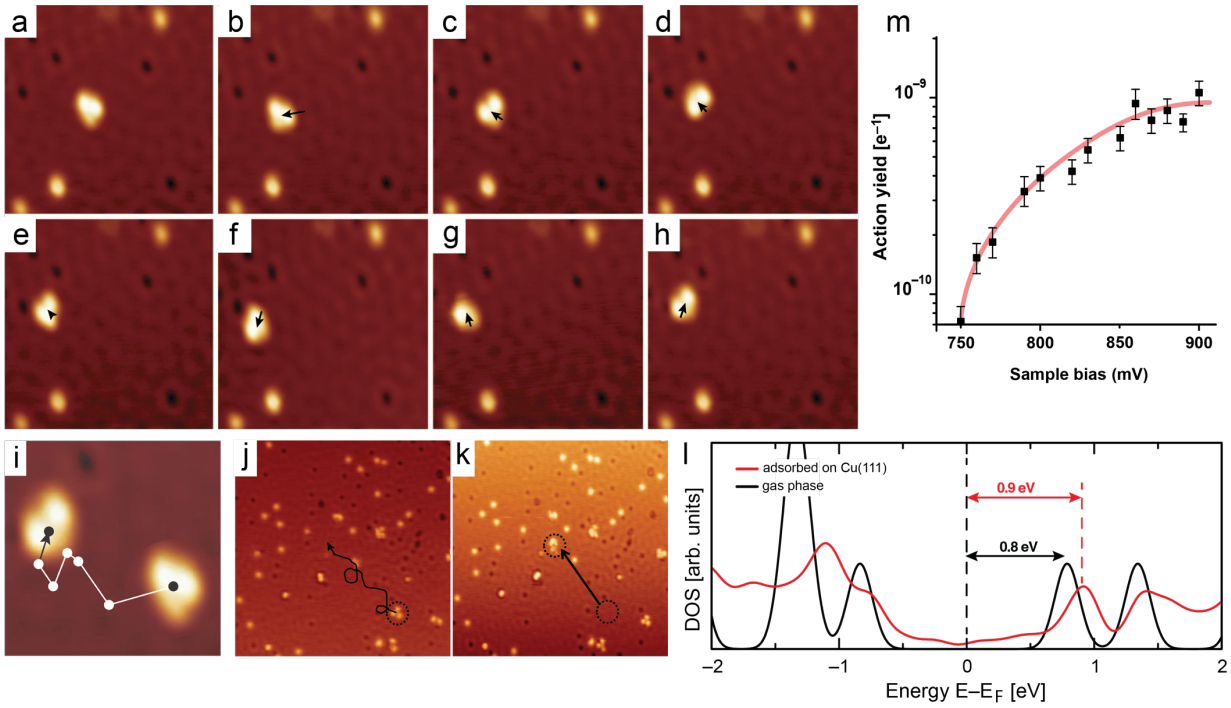

Figure 4. Movement of **1** across the Cu(111) surface due to injection of electrons. a-h) Sequence of STM images (15 nm × 15 nm, 50 mV, 10 pA) before and after injection of electrons in the center of the molecule between the three lobes at a bias voltage of 800 mV. The movements from the previous positions are indicated by arrows. Black dots represent CO molecules adsorbed on the surface. i) Composition of the initial and final STM images shown in a) and h) with the indication of the path taken from images a) to h). j) STM image (60 nm × 60 nm, 50 mV, 10 pA) before 60 manipulations of **1** at 800 mV bias voltage. The path of the molecule due to the 60 excitation steps is indicated. k) STM image (60 nm × 60 nm, 50 mV, 10 pA) after 60 manipulations of **1** at 800 mV bias voltage. The molecule moved 14 nm across the surface, as indicated by an arrow connecting initial and final position and the moving trajectory trace indicated in j). l) Calculated density of states for the free molecule (black trace) and of the molecule in the adsorbed state, including the states of the Cu(111) surface (red trace). For the free molecule LUMO and LUMO+1 are located at 0.8 eV and 1.3 eV, respectively. m) Plot of the yield of movement as function of

positive bias voltage (electrons tunneling from the STM tip into unoccupied surface states). The onset of this action at 750 meV correlates well with the onset of the unoccupied molecular states.

There is only a low degree of translational directionality observed (Figures 4i,j; S6-S8). Due to the C_2-symmetry of the free species overall directionality of the rotor may not be expected. However, the presence of the surface renders the methyl groups at the C5-ring core different (Figure 2a-c), thus creating a pseudo-asymmetric C-atom. This introduces an asymmetric PES and unidirectional rotation of the rotor units. Each of the two alkene groups experiences chirality with opposite helicity, and both fluorene groups rotate into the same direction with respect to the bridge unit.[51] This fact may explain why no pronounced backward movement and a modest overall directionality in the traces were observed (Figure 4i,j). However, directionality of the movement on the surface is expected to depend rather on which motor units become excited in a sequence of excitations. If the same side is successively put into action, straight forward movement cannot be expected. In the case of the nanocar, its four rotors lower substantially the probability of consecutive excitation of the same rotor, leading to the large degree of directionality.

Movement across the surface is not limited to the formation of a transient anion upon adding an electron to the LUMO. Inelastic tunneling excitation can excite a HOMO electron just into unoccupied states of the metal substrate above the Fermi level, and such hole formation may induce the process of *E*-*Z* isomerization. Upon optical excitation of a free molecule a hole is created in the HOMO, while the electron occupies the LUMO (then called SUMO). Such relocation of charge increases dramatically the anti-bonding character, leading to the *E*-*Z* isomerization. However, it has been shown for single hole cations or SUMO anions, that the double bond character is lowered sufficiently in order to initialize *E*-*Z* isomerization.[58-60]

As the metal electrons near the Fermi level tend to quickly quench excited states, it would be interesting to see if more pronounced motor action can be observed on semiconductor surfaces. However, larger band gaps will then require much higher bias voltages for sufficient electron tunneling than needed for vibrational excitation.[44]

CONCLUSIONS

In summary, it has been shown that inelastic electron tunneling efficiently induces vibrational excitation, leading to conformational switching of the helical units in the sterically overcrowded motor molecule. IET electronic excitation causes *E-Z* isomerization that leads to rotation of one of the two rotor units and to movement of the molecule across the copper surface.

METHODS

Materials preparation

1,3-Difluoreno-2,2,3,6-tetramethyl indene (Figure 1, $C_{36}H_{30}$, **1**) has been synthesized as described in detail previously.[49] The copper single-crystal surface was cleaned *in-vacuo* using standard preparation techniques, that is, by argon cation bombardment and healed by annealing at elevated temperatures. The molecules were sublimed from a home-built evaporator, at 368 K on a cold sample held at 32 K. The Cu(111) crystal temperature was 5 K during imaging.

STM experiments

All STM images presented here were recorded in constant-current mode with a sample bias of 50 mV and a tunneling current of 10 pA. Switching and molecular motion was induced by applying a voltage pulse to the sample while the tunneling current was recorded. The STM tip was positioned over the center of a molecule, the feedback was turned off, and the tip was moved vertically to give the desired initial current during the pulse.

Density functional theory (DFT)

DFT calculation of the surface **(*P*)-1** conformation (Figure S3) was performed with an optB86-vdW functional, which accounts for dispersion effects, and ultrasoft pseudo-potentials as implemented in the Quantum Espresso package (http://www.quantum-espresso.org/). The single-particle electronic wave functions and charge densities were expanded in a plane-wave basis set, up to an energy cutoff of 25 Ry and 250 Ry, respectively. An isolated molecule on the surface was considered, where a periodic four-atom-layer slab consisting of 440 Cu atoms and a vacuum space of 23 Å perpendicular to the surface direction was used. Dipole corrections along the direction perpendicular to the metal surface area were applied. Structural relaxations have been performed at the GAMMA point with the bottom two layers fixed and all other atoms allowed to relax unconstrained until the forces on each atom are less than 0.013 eV/Å.

Hybrid DFT/molecular mechanics calculations

Simulations of conformations (Figures 2 and S3) were performed using a QM/MM method, i.e., Fireball/Amber,[61] that combines interface force field[62] for the Cu surface with Fireball local orbital DFT[63] for the molecule. Fireball calculations used the BLYP exchange-correlation functional[64,65] with D3 corrections[66] and norm-conserving pseudopotentials together with a basis set of optimized numerical atomic-like orbitals,[67] *s* for H and sp^3 for C. For each possible structure of the molecule a QM/MM MD simulation of 100 ps with a time step of 0.5 fs at a temperature of 100 K was performed, followed by a final relaxation where the interaction energy and the orbitals were calculated.

STM image calculations

Constant-current STM simulations were performed using Density Functional Theory and the Probe Particle Scanning Probe Microscopy (PPSTM) code.[68] Unlike the Tersoff-Haman approach which only employs the electronic structure of the sample, the PPSTM method makes use of

Bardeen's approach to the theory of tunneling probability which depends on the distance of tip and sample as well as electronic state of the tip. In the PPSTM constant-current mode, first the tunneling current over a selected 3D scanning grid in real space is calculated. Then for a selected value of current, the z-coordinates are plotted as 2D maps for every x and y coordinate of the sampling grid.

For the different principle conformation different strained structures were calculated by rotation of the indeno groups with respect to middle part of the molecule. The free energy profile has been calculated using WHAM methodology[69] with MD at 50 K and the dihedral angle between C-C bonds at the alkene group as the reaction coordinate.

ASSOCIATED CONTENT

Supporting Information.

STM images showing conformational switching and trajectories of movement; results of theoretical structure determination and STM contrast modelling.

AUTHOR INFORMATION

Present Addresses

PS: Department of Chemistry, University of Zurich, Winterthurerstrasse 190, 8057 Zürich, Switzerland

JCMK: Centre for Organic Photonics & Electronic, School of Chemistry and Molecular Biosciences, The University of Queensland, Queensland 4072, Australia

JIMM: Departamento de Física de la Materia Condensada and Condensed Matter Physics Center (IFIMAC), Universidad Autónoma de Madrid, ES-28049, Madrid, Spain

Author Contributions

The manuscript was written through contributions of all authors. All authors have given approval to the final version of the manuscript.

Funding Sources

Swiss National Science Foundation - grant 163296

Czech Science Foundation grant No. 21-17194L

European Research Council ERC; advanced grant No.694345

Dutch Ministry of Education, Culture and Science (Gravitation program No.024.001.035 BLF)

Notes

ACKNOWLEDGMENT

Support by the Swiss National Science Foundation (grant 163296) is gratefully acknowledged. Financial support from the European Research Council (ERC; advanced grant No.694345 to B.L.F.), and the Dutch Ministry of Education, Culture and Science (Gravitation program No.024.001.035 BLF) is gratefully acknowledged. This work was supported by the Czech Science Foundation grant No. 21-17194L.

REFERENCES

(1) Molecular Motors; Schliwa, M., Ed.; Wiley-VCH: Weinheim, 2003.

(2) Sauvage, J. P. From Chemical Topology to Molecular Machines (Nobel Lecture). *Angew. Chem. Int. Ed.* **2017**, *56*, 11080–11093.

(3) Stoddart, J. F. Mechanically Interlocked Molecules (MIMs)—Molecular Shuttles, Switches, and Machines (Nobel Lecture). *Angew. Chem. Int. Ed.* **2017**, *56*, 11094–11125.

(4) Feringa, B. L. The Art of Building Small: From Molecular Switches to Motors (Nobel Lecture). *Angew. Chem. Int. Ed.* **2017**, *56*, 11060–11078.

(5) Erbas-Cakmak, S.; Leigh, D. A.; McTernan, C. T.; Nussbaumer, A. L. Artificial Molecular Machines. *Chem. Rev.* **2015**, *115*, 10081–10206.

(6) Balzani, V.; Credi, A.; Raymo, F.; Stoddart, J. F. Artificial Molecular Machines. *Angew. Chem. Int. Ed.* **2000**, *39*, 3348–3391.

(7) From Non-Covalent Assemblies to Molecular Machines; Sauvage, J.-P., Gaspard, P., Eds.; Wiley-VCH: Weinheim; 2010.

(8) The Nature of the Mechanical Bond: From Molecules to Machines; Bruns, C. J., Stoddart, J. F., Eds.; Wiley-VCH: Weinheim; 2016.

(9) Browne, W. R.; Feringa, B. L. Making Molecular Machines Work. *Nat. Nanotechnol.* **2006**, *1*, 25–35.

(10) Greb, L.; Lehn, J.-M. Light-Driven Molecular Motors: Imines as Four-Step or Two-Step Unidirectional Rotors. *J. Am. Chem. Soc.* **2014**, *136*, 13114–13117.

(11) Kassem, S.; van Leeuwen, T.; Lubbe, A. S.; Wilson, M. R.; Feringa, B. L.; Leigh, D. A. Artificial Molecular Motors. *Chem. Soc. Rev.* **2017**, *46*, 2592–2621.

(12) García-López, V.; Liu, D.; Tour, J. M. Light-Activated Organic Molecular Motors and Their Applications. *Chem. Rev.* **2020**, *120*, 79–124.

(13) Astumian, R. D. Design Principles for Brownian Molecular Machines: How to Swim in Molasses and Walk in a Hurricane. *Phys. Chem. Chem. Phys.* **2007**, *9*, 5067–5083.

(14) Dattler, D.; Fuks, G.; Heiser, J.; Moulin, E.; Perrot, A.; Yao, X.; Giuseppone, N. Design of Collective Motions from Synthetic Molecular Switches, Rotors, and Motors. *Chem. Rev.* **2020**, *120*, 1, 310–343.

(15) Baroncini, M.; Silva, S.; Credi, A. Photo- and Redox-Driven Artificial Molecular Motors. *Chem. Rev.* **2020**, *120*, *1*, 200–268.

(16) Koumura, N.; Zijlstra, R. W. J.; van Delden, R. A.; Harada, N.; Feringa, B. L. Light-Driven Monodirectional Molecular Rotor. *Nature* **1999**, *401*, 152–155.

(17) Cnossen, A.; Browne, W. R.; Feringa, B. L. Unidirectional Light-Driven Molecular Motors Based on Overcrowded Alkenes. *Top. Curr. Chem.* **2014**, *354*, 139–162.

(18) Eelkema, R.; Pollard, M. M.; Vicario, J.; Katsonis, N.; Ramon, B. S.; Bastiaansen, C. W. M.; Broer, D. J.; Feringa, B. L. Nanomotor Rotates Microscale Objects. *Nature* **2006**, 440,163–163.

(19) Marchand, G.; Eng, J.; Schapiro, I.; Valentini, A.; Frutos, L. M.; Pieri, E.; Olivucci, M.; Léonard, J.; Gindensperger, E. Directionality of Double-Bond Photoisomerization Dynamics Induced by a Single Stereogenic Center. *J. Phys. Chem. Lett.* **2015**, *6*, 599–604.

(20) Feringa, B. L.; Jager, W. F.; de Lange, B.; Meijer, E. W. Chiroptical Molecular Switch. *J. Am. Chem. Soc.* **1991**, *113*, 5468–5470.

(21) Augulis, R.; Klok, M.; Feringa, B. L.; Loosdrecht, P. H. M. V. Light-Driven Rotary Molecular Motors: An Ultrafast Optical Study *Phys. Status Solidi C* **2009**, *6*, 181–184.

(22) Leigh, D. A.; Wong, J. K. Y.; Dehez, F.; Zerbetto, F. Unidirectional Rotation in a Mechanically Interlocked Molecular Rotor. *Nature* **2003**, *424*, 174–179.

(23) Hernández, J. V.; Kay, E. R.; Leigh, D. A. A Reversible Synthetic Rotary Molecular Motor. *Science* **2004**, *306*, 1532–1537.

(24) Fletcher, S. P.; Dumur, F.; Pollard, M. M.; Feringa, B. L. A Reversible, Unidirectional Molecular Rotary Motor Driven by Chemical Energy. *Science* **2005**, *310*, 80–82.

(25) Collins, B. S. L.; Kistemaker, J. C. M.; Otten, E.; Feringa, B. L. A Chemically Powered Unidirectional Rotary Molecular Motor Based on a Palladium Redox Cycle. *Nat. Chem*. **2016**, *8*, 860–866.

(26) Zhang, Y.; Chang, Z.; Zhao, H.; Crespi, S.; Feringa, B. L.; Zhao, D. P. A Chemically Driven Rotary Molecular Motor Based on Reversible Lactone Formation with Perfect Unidirectionality. *Chem.* **2020**, *6*, 2420–2429.

(27) Binnig, G.; Rohrer, H.; Gerber, C.; Weibel, E. Surface Studies by Scanning Tunneling Microscopy. *Phys. Rev. Lett.* **1982**, *49*, 57–61.

(28) Eigler, D. M.; Schweizer, E. K. Positioning Single Atoms with a Scanning Tunneling Microscope. *Nature* **1990**, *344*, 524–526.

(29) Morgenstern, K.; Lorente, N.; Rieder, K.-H. Controlled Manipulation of Single Atoms and Small Molecules. *Phys. Status Solidi B* **2013**, *250*, 1671–1751.

(30) Böhringer, M.; Morgenstern, K.; Schneider, W.-D.; Berndt, R. Separation of a Racemic Mixture of Two-Dimensional Molecular Clusters by Scanning Tunneling Microscopy. *Angew. Chem. Int. Ed.* **1999**, *38*, 821–823.

(31) Ernst, K.-H.; Baumann, S.; Lutz, C. P.; Seibel, J.; Zoppi, L.; Heinrich, A. J. Pasteur's Experiment Performed at the Nanoscale: Manual Separation of Chiral Molecules, One by One. *Nano Lett.* **2015**, *15*, 5388–5392.

(32) Komeda, T.; Kim, Y.; Kawai, M. Persson, B. N. J.; Ueba, H. Lateral Hopping of Molecules Induced by Excitation of Internal Vibration Mode. *Science* **2002**, *295*, 2055–2058.

(33) Parschau, M.; Passerone, D.; Rieder, K.-H.; Hug, H. J.; Ernst K.-H. Switching the Chirality of Single Adsorbate Complexes. *Angew. Chem. Int. Ed.* **2009**, *48*, 4065–4068.

(34) Ho, W. Single-Molecule Chemistry. *J. Chem. Phys.* **2002**, *117*, 11033–11061.

(35) Kim, Y.; Motobayashi, K.; Frederiksen, T.; Ueba, H.; Kawai, M. Action Spectroscopy for Single-Molecule Reactions – Experiments and Theory. *Prog. Surf. Sci.* **2015**, *90*, 85–143.

(36) Stipe, B. C.; Rezaei, M. A.; Ho, W. Coupling of Vibrational Excitation to the Rotational Motion of a Single Adsorbed Molecule. *Phys. Rev. Lett.* **1998**, *81*, 1263–1266.

(37) Natterer, F. D.; Patthey, F.; Brune, H. Resonant-Enhanced Spectroscopy of Molecular Rotations with a Scanning Tunneling Microscope. *ACS Nano* **2014**, *8*, 7099–7105.

(38) Pascual, J. I.; Lorente, N.; Song, Z.; Conrad, H.; Rust, H. P. Selectivity in Vibrationally Mediated Single-Molecule Chemistry. *Nature* **2003**, *423*, 525–528.

(39) Kim, Y.; Komeda, T.; Kawai, M. Single-Molecule Reaction and Characterization by Vibrational Excitation. *Phys. Rev. Lett.* **2002**, *89*, 126104/1–4.

(40) Hla, S.-W.; Rieder, K.-H. STM Control of Chemical Reactions: Single-Molecule Synthesis. *Annu. Rev. Phys. Chem.* **2003**, *54*, 307–330.

(41) Parschau, M.; Rieder, K.-H.; Hug, H. J.; Ernst, K.-H. Single-Molecule Chemistry and Analysis: Mode-Specific Dehydrogenation of Adsorbed Propene by Inelastic Electron Tunneling. *J. Am. Chem. Soc.* **2011**, *133*, 5689–5691.

(42) Henzl, J.; Mehlhorn, M.; Gawronski, H.; Rieder, K.-H.; Morgenstern, K. Reversible Cis-Trans Isomerization of a Single Azobenzene Molecule. *Angew. Chem. Int. Ed.* **2006**, *45*, 603–606.

(43) Perera, U. G. E.; Ample, F.; Kersell, H.; Zhang, Y.; Vives, G.; Echeverria, J.; Grisolia, M.; Rapenne, G.; Joachim, C.; Hla, S. W. Controlled Clockwise and Anticlockwise Rotational Switching of a Molecular Motor. *Nat. Nanotechnol.* **2013**, *8*, 46–51.

(44) Jacobson, P.; Prezzi, D.; Liu, D.; Schied, M.; Tour, J. M.; Corni, S.; Calzolari, A.; Molinari, E.; Grill, L. Adsorption and Motion of Single Molecular Motors on TiO_2(110). *J. Phys. Chem. C* **2020**, *124*, 24776–24785.

(45) Tierney, H. L.; Murphy, C. J.; Jewell, A. D.; Baber, A. E.; Iski, E. V.; Khodaverdian, H. Y.; McGuire, A. F.; Klebanov, N.; Sykes, E. C. H. Experimental Demonstration of a Single-Molecule Electric Motor. *Nat. Nanotechnol.* **2011**, *6*, 625–629.

(46) Balema, T. A.; Liu, Y.; Wasio, N. A.; Larson, A. M.; Patel, D. A.; Deshlahra, P.; Sykes, E. C. H. Enantioselective Effects in the Electrical Excitation of Amine Single-Molecule Rotors. *J. Phys. Chem. C* **2021,** *125*, 3584–3589.

(47) Stolz, S.; Gröning, O.; Prinz, J.; Brune, H.; Widmer, R. Molecular Motor Crossing the Frontier of Classical to Quantum Tunneling Motion. *PNAS* **2020**, *117*, 14838–14842.

(48) Pollard, M. M.; ter Wiel, M. K. J.; van Delden, R. A.; Vicario, J.; Koumura, N.; van den Brom, C. R.; Meetsma, A.; Feringa, B. L. Light-Driven Rotary Molecular Motors on Gold Nanoparticles. *Chem. Eur. J.* **2008**, *14*, 11610–11622.

(49) Saywell, A.; Bakker, A.; Mielke, J.; Kumagai, T.; Wolf, M.; García-López, V.; Chiang, P.-T.; Tour, J. M.; Grill, L. Light-Induced Translation of Motorized Molecules on a Surface. *ACS Nano* **2016**, *10*, 10945–10952.

(50) Kudernac, T.; Ruangsupapichat, N.; Parschau, M.; Maciá, B.; Katsonis, N.; Harutyunyan, S. R.; Ernst, K.-H. ; Feringa, B. L. Electrically Driven Directional Motion of a Four-Wheeled Molecule on a Metal Surface. *Nature* **2011**, *479*, 208–211.

(51) Kistemaker, J. C. M.; Štacko, P.; Roke, D. ;Wolters, A. T.; Heideman, G. H.; Chang, M.-C.; van der Meulen, P.; Visser, J.; Otten, E.; Feringa, B. L. Third-Generation Light-Driven Symmetric Molecular Motors. *J. Am. Chem. Soc.* **2017**, *139*, 9650–9661.

(52) Kistemaker, J. C. M.; Štacko, P.; Visser, Feringa, B. L. Unidirectional Rotary Motion in Achiral Molecular Motors. *Nat. Chem.* **2015**, *7*, 890—896.

(53) Lu, H.-L.; Cao, Y.; Qi, J.; Bakker, A.; Strassert, C. A.; Lin, X.; Ernst, K.-H.; Du, S.; Fuchs, H.; Gao, H.-J. Modification of the Potential Landscape of Molecular Rotors on Au(111) by the Presence of an STM Tip. *Nano Lett.* **2018**, *18*, 4704–4709.

(54) Gehrig, J. C.; Penedo, M.; Parschau, M.; Schwenk, J.; Marioni, M. A.; Hudson, E. W.; Hug, H. J. Surface Single-Molecule Dynamics Controlled by Entropy at Low Temperatures. *Nat. Commun.* **2017**, *8*, 14404/1–8

(55) Tully, J. C. Chemical Dynamics at Metal Surfaces. *Annu. Rev. Phys. Chem.* **2000**, *51*, 153–178.

(56) Ueba, H.; Passerone, D.; Parschau, M.; Ernst, K. H. Action Spectroscopy Associated With Inelastic Two-Electron Tunneling of a Single Molecule: Propene on Cu(211). *Surf. Sci.* **2018**, *678*, 206–214.

(57) Hall, C. R.; Conyard, J.; Heisler, I. A.; Jones, G.; Frost, J.; Browne, W. R.; Feringa, B. L.; Meech, S. R. Ultrafast Dynamics in Light-Driven Molecular Rotary Motors Probed by Femtosecond Stimulated Raman Spectroscopy. *J. Am. Chem. Soc.* **2017**, *139*, 7408–7414.

(58) Füchsel, G.; Klamroth, T.; Dokić, J.; Saalfrank, P. On the Electronic Structure of Neutral and Ionic Azobenzenes and Their Possible Role as Surface Mounted Molecular Switches. *J. Phys. Chem. B* **2006**, *110*, 16337–16345.

(59) Schmidt, R.; Hagen, S.; Brete, D.; Carley, R.; Gahl, C.; Dokić, J.; Saalfrank, P.; Hecht, S.; Tegeder, P.; Weinelt, M. On the Electronic and Geometrical Structure of the Trans- And Cis-Isomer of Tetra-Tert-Butyl-Azobenzene on Au(111). *Phys. Chem. Chem. Phys.* **2010**, *12*, 4488–4497.

(60) Leyssner, F.; Hagen, S.; Óvári, L.; Dokić, J.; Saalfrank, P.; Peters, M. V.; Hecht, S.; Klamroth, T.; Tegeder, P. Photoisomerization Ability of Molecular Switches Adsorbed on Au(111): Comparison between Azobenzene and Stilbene Derivatives. *J. Phys. Chem. C* **2010**, *114*, 1231–1239.

(61) Mendieta-Moreno, J. I.; Walker, R. C.; Lewis, J. P.; Gómez-Puertas, P.; Mendieta, J.; Ortega, J. FIREBALL/AMBER: An Efficient Local-Orbital DFT QM/MM Method for Biomolecular Systems. *J. Chem. Theory Comput.* **2014**, *10*, 2185–2193.

(62) Heinz, H.; Lin, T. J.; Kishore Mishra, R.; Emami, F. S. Thermodynamically Consistent Force Fields for the Assembly of Inorganic, Organic, and Biological Nanostructures: The INTERFACE Force Field *Langmuir* **2013**, *29*, 1754–1765.

(63) Lewis, J. P.; Jelinek, P.; Ortega, J.; Demkov, A. A.; Trabada, D. G.; Haycock, B.; Wang, H.; Adams, G.; Tomfohr, J. K.; Abad, E.; Wang, H.; Drabold, D. A. Advances and applications in the FIREBALL ab initio tight-binding molecular-dynamics formalism. *Phys. Status Solidi B* **2011**, *248*, 1989–2007.

(64) Becke, A. D. Density-Functional Exchange-Energy Approximation With Correct Asymptotic Behavior. *Phys. Rev. A* **1988**, *38*, 3098–3100.

(65) Lee, C.; Yang, W.; Parr, R. G. Development of the Colle-Salvetti Correlation-Energy Formula Into a Functional of the Electron Density. *Phys. Rev. B* **1988**, *37*, 785–789.

(66) Grimme, S.; Ehrlich, S.; Goerigk, L. Effect of the Damping Function in Dispersion Corrected Density Functional Theory. *J. Comput. Chem.* **2011**, *32*, 1456–1465.

(67) Basanta, M.; Dappe, Y. J.; Jelinek, P.; Ortega, J. Optimized Atomic-Like Orbitals for First-Principles Tight-Binding Molecular Dynamics. *Comput. Mater. Sci.* **2007**, *39*, 759–766.

(68) Krejčí, O.; Hapala, P.; Ondráček, M.; Jelínek, P. Principles and simulations of high-resolution STM imaging with a flexible tip apex. *Phys. Rev. B* **2017**, *95*, 045407/1–9.

(69) Kumar, S.; Rosenberg, J. M.; Bouzida, D.; Swendsen, R. H.; Kollman, P. A. The Weighted Histogram Analysis Method for Free-Energy Calculations on Biomolecules. I. The Method. *J. Comput. Chem.* **1992**, *13*, 1011–1021.

TOC graphics